Interstitial point radiance spectroscopy of turbid media

Lee C. L. Chin,[1,a)] Brendan Lloyd,[2] William M. Whelan,[2,4,6] and I. Alex Vitkin[2,3,5]
[1]*Department of Medical Physics, Odette Cancer Centre, Toronto M4N 3M5, Canada*
[2]*Department of Medical Biophysics, University of Toronto, Toronto M5G 2M9, Canada*
[3]*Department of Radiation Oncology, University of Toronto, Toronto M5G 2M9, Canada*
[4]*Department of Physics, Ryerson University, Toronto M5B 2K3, Canada*
[5]*Division of Biophysics and Bioimaging, Ontario Cancer Institute/University Health Network, Toronto M5G 2M9, Canada*
[6]*Department of Physics, University of Prince Edward Island, Charlottetown, Prince Edward Island C1A 4P3, Canada*

(Received 14 April 2008; accepted 8 December 2008; published online 19 May 2009)

We present an optical technique, point radiance spectroscopy, to directly recover chromophore concentrations and the reduced optical scattering coefficient spectrum from continuous wave interstitial point radiance measurements at a single-source-detector separation in turbid, tissuelike media. The method employs a spectral algorithm to fit the relative radiance data, using the P3 approximation, at only two detection angles (0° and 90°). The spectral fitting algorithm is applied to simulated data of relative point fluence and relative point radiance data with added 1% noise and shows that even under realistic experimental conditions, only point radiance information is able to provide quantitative information regarding chromophore concentrations and scattering power at distances greater than two to three mean free paths from the source. Furthermore, experimental measurements in tissue-simulating phantoms demonstrate that dye concentrations and scattering parameters can be recovered to within ~10%. The developed point radiance technique bridges a technological gap between local surface reflectance and spatially resolved interstitial fluence methods in optical assessment of random media such as biological tissue. © *2009 American Institute of Physics*. [DOI: 10.1063/1.3116132]

I. INTRODUCTION

Diffuse interstitial spectroscopy is currently under investigation to optically assess drug concentrations during photodynamic therapy,[1] areas of thermal damage following thermal ablation,[2] or diagnosis of cancerous tissues.[3] Of particular interest is the quantitative determination of known endogenous and exogenous absorbers (i.e., chromophores), as well as information regarding the scattering properties of tissues.

Spatially resolved continuous wave (cw) fluence measurements are the most common means for determining tissue optical properties under interstitial geometry. In this method fluence $\phi(r)$ acquired at multiple known radial distances, r, from a point source is analyzed using the diffusion approximation of the radiative transfer equation (RTE) to evaluate the bulk effective attenuation coefficient, μ_{eff}, of the tissue of interest. Assessment of μ_{eff} at multiple wavelengths in combination with spectral fitting algorithms allows one to derive information regarding the chromophore concentrations and scattering properties of the interrogated medium. Spectral fitting algorithms, adopted by a number of groups, restrict the absorption coefficient as a function of wavelength, $\mu_a(\lambda)$, to a limited range of known spectral shapes based on reasonable assumptions regarding the dominant chromophores of interest in the medium.[1,4,5] Previous work by Zhu *et al.*[1] utilized relative fluence scans at *multiple* positions and spectral constraints to recover chromophore concentrations. However, considerable variability in tissue properties is often observed not only among patients but even within an individual.[1] Techniques that provide localized assessment of chromophore concentrations may allow for more accurate assessment of tissue status. This is a potential weakness of current interstitial fluence methods due to the large volume interrogated during a spatially resolved $\phi(r)$ scan.

One approach for improving spatial resolution is to minimize the number of source-detector positions employed in the measurements. This idea has motivated considerable investigation[3,4,6] on the development of local reflectance techniques to address the highly heterogeneous nature of tissue. Unlike the fluence method described above, these techniques measure the reflected light intensity at one or two short distances (<1 mm) from a plane-cut source. The source and detection fibers are bundled into a single needle probe that is inserted interstitially into the region of interest. Due to the close proximity of the fibers the interrogated area is generally confined to depths of 100–200 μm, thereby allowing for tissue characterization proximal to the probe surface. However, these methods suffer from the same concerns of conventional needle biopsies in that inaccurate positioning of the probe tip outside the diseased region will lead to false negative biopsy assessments.

An optimal tissue characterization would balance the *larger* sampling volumes offered by spatially resolved fluence methods with the localized assessment afforded by the interstitial reflectance methods. Such a compromise could be achieved by developing an interstitial technique that requires only a single-source-detector position that is not restricted to

a)Electronic mail: leecl.chin@gmail.com.

close source-detector separations. Although time- or frequency-domain methods may satisfy such criteria, the instrumentation is significantly more costly than cw measurements.

A potential steady-state alternative to time-domain methods, recently reported by Xu *et al.*,[7] is to employ reasonable assumptions of the water concentration of tissue and employ a second-differential analysis (SDA) of the transmission spectrum at multiple wavelengths to estimate the pathlength of the traveled photons. Since, like time-domain methods, the pathlength is obtained directly, only a single-source detector is required to obtain quantitative information regarding chromophore content. However, while promising, the method still requires measurements at multiple source-detector separations to obtain information regarding tissue scattering. Furthermore, because of the reliance of the SDA on knowledge of water content, the method is particularly sensitive to inhomogeneities in water concentration or when the water concentration is incorrectly estimated. While it has been suggested that magnetic resonance (MR) imaging may be employed to provide the additional information of water heterogeneities, the high cost of MR imagers makes the SDA approach impractical for routine on-line monitoring of low-cost interstitial therapies or routine optical biopsy of suspicious masses.

Alternatively, relative directional light intensity or radiance measurements have been investigated as a potential single point detection method for interstitial settings.[8,9] Unlike fluence data, radiance measurements examine the light intensity impinging on a single spatial position from multiple detection angles (directions) relative to the source. Note that integration of the radiance over all polar and azimuthal angles yields fluence. The method, initially demonstrated by Dickey *et al.*[8] at a single discrete wavelength, was further examined by Chin *et al.*[9] who verified the uniqueness of point radiance data by examining chi-square, χ^2, contours of relative radiance data for various property sets, detection angles, and sensor positions.

Here we further demonstrate the ability of relative radiance data at a *single position* to retrieve information regarding tissue chromophore concentrations and scattering spectra by extending the technique to multiple wavelengths. Instead of measurements at multiple detection angles, we employ the simpler ratio between only *two* detection angles, $L_r = L(90°)/L(0°)$, and utilize spectral constraints to directly recover chromophore and scattering information. The detection angles were chosen to maximize signal to noise ratio, minimize experimental complexities, and ensure uniqueness in the recovery (inversion) process of optical properties.[9] We hypothesize that the increased information content of spectral radiance measurements, combined with spectral constraints, would stabilize the inversion process and improve accuracy even with reduced data of limited detection angles.

This paper is structured as follows. In Sec. II, we derive equations demonstrating the uniqueness of spectrally constrained point radiance measurements from the diffusion approximation for light transport in tissue. The materials and methods employed in this work are also described. In Sec. III, simulations are employed to illustrate the strength of the radiance technique by comparing the ability of both relative *point* fluence and relative point radiance data to retrieve absolute chromophore concentration and scattering parameters. Experimental verification of the approach to retrieve dye concentrations and scattering parameters is performed in tissue-simulating phantoms. We conclude with a discussion and summary of our results.

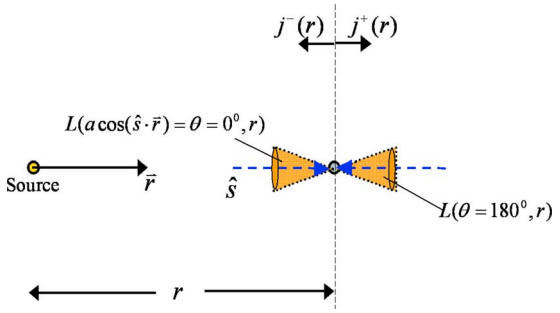

FIG. 1. (Color online) Radiance geometry for a point source in a turbid optical medium of infinite extent.

II. METHODS

A. Uniqueness of spectrally constrained point radiance measurements

We first illustrate our approach under conditions of linear anisotropy of the light field in tissue (also known as diffusion approximation), and then discuss how the method can be extended to higher degrees of anisotropy. Consider an isotropically emitting steady-state single wavelength point source in an infinite homogeneous volume with reduced scattering coefficient μ_s' and absorption coefficient μ_a (Fig. 1). In the diffusion approximation, the radiance (directional light intensity), $L(r,\hat{\Omega})$, at a known position, r, and within solid angle, $\hat{\Omega}$, is described as a sum of an isotropic component (the fluence rate) $\phi(r)=(P_o/4\pi Dr)\exp(-\mu_{\text{eff}}r)$ and a directional component (the diffuse flux) $j(r)=-D\nabla\phi(r)$:

$$L(r,\hat{\Omega}) = \frac{1}{4\pi}\phi(r) + \frac{3}{4\pi}j(r)\cdot\hat{\Omega}$$

$$= \frac{P_o}{4\pi}\frac{1}{4\pi rD}[1+3(D/r+\sqrt{\mu_a D})\cos\theta]e^{-\mu_{\text{eff}}r}, \quad (1)$$

where D is the diffusion coefficient $(=1/3\mu_s')$ under conditions of low absorption), $\mu_{\text{eff}}=\sqrt{\mu_a/D}$ is the effective attenuation coefficient, and P_o is the source power.[10] Here, $j(r)\cdot\hat{\Omega}$ is a function of $\cos\theta$, where $\theta=0°$ faces the light source and $\theta=180°$ faces away from the source. Integration of the radiance over all solid angles yields the fluence and clearly results in a loss of directional information.

Here we take advantage of the added information content of radiance measurements to uniquely determine spectral parameters using a single optode pair.

During spectroscopic assessment, the quantities of interest are the chromophore (i.e., oxy- and deoxyhemoglobin and water) concentrations, ε, and the bulk scattering parameters (i.e., scattering power and wavelength dependence).

The absorption spectra of biological chromophores carry distinct spectral features. However, due to the diverse range of scatterer shapes and sizes in biological tissues, multiple scattering events result in a virtually featureless scattering spectrum that decreases monotonically as a function of wavelength. Various investigators[4,11] have demonstrated that scattering in biological tissues can be well described by a simple power law equation given by $\mu_s'(\lambda) \sim A\lambda^{-b}$, where A reflects the scattering cross section and b, which is related to the scatterer spacing, describes the rate of spectral decrease. Note that the form of this equation is dimensionally inconsistent and is used here only for simplicity in the derivation. A more dimensionally accurate form is presented in Sec. II C.

For a given position r and wavelength λ, taking the ratio of the radiance at two *different* detection angles ($\theta=0°$ and 90°) yields the *relative* radiance, $L_{\mathrm{rel}}(r,\lambda)$:

$$L_{\mathrm{rel}}(r,\lambda) = \frac{L(r,0°)}{L(r,90°)} = 1 + \frac{1}{A\lambda^{-b}}\left(\frac{1}{r} + \mu_{\mathrm{eff}}(\lambda)\right). \tag{2}$$

In Eq. (2) we have introduced the power law dependence for diffuse media.[8] $L_{\mathrm{rel}}(r,\lambda)$ is a measure of the anisotropy of the light field at a given wavelength and changes with the albedo of the interrogated medium.

If $L_{\mathrm{rel}}(r,\lambda)$ is measured at two wavelengths, λ_1 and λ_2, Eq. (2) yields four unknown quantities: A, b, $\mu_{\mathrm{eff}}(\lambda_1)$, and $\mu_{\mathrm{eff}}(\lambda_2)$, which are related to the experimental measurements $L_{\mathrm{rel}}(r,\lambda_1)$ and $L_{\mathrm{rel}}(r,\lambda_2)$ by

$$\mu_{\mathrm{eff}}(\lambda_2) - \mu_{\mathrm{eff}}(\lambda_1) = A(\lambda_2^{-b}[L_{\mathrm{rel}}(\lambda_2) - 1] - \lambda_1^{-b}[L_{\mathrm{rel}}(\lambda_1) - 1]). \tag{3}$$

Note that A and b are *independent* of wavelength.

Alternatively, for a *fixed* detection angle (here, for simplicity $\theta=90°$), we can take the ratio of the radiance at two different wavelengths, λ_1 and λ_2, to give the relative wavelength attenuation, $\kappa_r(r,\lambda_1,\lambda_2)$:

$$\kappa_r(r,\lambda_1,\lambda_2) = \frac{L(90°,\lambda_1)}{L(90°,\lambda_2)} = \frac{\lambda_2^b}{\lambda_1^b} e^{[\mu_{\mathrm{eff}}(\lambda_2)-\mu_{\mathrm{eff}}(\lambda_1)]r}. \tag{4}$$

$\kappa_r(r,\lambda_1,\lambda_2)$ is analogous to relative attenuation data obtained using the more commonly employed fluence measurements.

Equation (4) can also be rearranged to isolate for $\mu_{\mathrm{eff}}(\lambda_1)$ and $\mu_{\mathrm{eff}}(\lambda_2)$ giving

$$\mu_{\mathrm{eff}}(\lambda_2) - \mu_{\mathrm{eff}}(\lambda_1) = \ln\left(\kappa_r(r,\lambda_1,\lambda_2)\frac{\lambda_1^b}{\lambda_2^b}\right)\frac{1}{r}. \tag{5}$$

Both $L_{\mathrm{rel}}(r,\lambda)$ (albedo dependence) and $\kappa_r(r,\lambda_1,\lambda_2)$ (attenuation dependence) provide distinct and separate information of the medium's optical properties.

Now, by inserting Eq. (3) into Eq. (5) we arrive at an expression that provides a unique solution to the medium's spectral scattering properties:

$$A = \frac{\ln\left(\kappa_r(r,\lambda_1,\lambda_2)\frac{\lambda_1^b}{\lambda_2^b}\right)}{r(\lambda_2^{-b}[L_{\mathrm{rel}}(\lambda_2) - 1] - \lambda_1^{-b}[L_{\mathrm{rel}}(\lambda_1) - 1])}. \tag{6}$$

Equation (6) describes the scattering parameters A and b *solely* as a function of the *measurements* $L_{\mathrm{rel}}(r,\lambda)$ and $\kappa_r(r,\lambda_1,\lambda_2)$ *without* any dependence on the absorption properties of the medium [contained in $\mu_{\mathrm{eff}}(\lambda_1)$ and $\mu_{\mathrm{eff}}(\lambda_2)$]. Equation (6) can be evaluated using multiple wavelength pairs (i.e., $[\lambda_1,\lambda_3]$, $[\lambda_2,\lambda_3]$, $[\lambda_3,\lambda_4]$,…) to arrive at a unique solution for both A and b. In practice, the stability and uniqueness of the inverse problem improve with additional spectral measurements and wavelength separation. With large spectral data sets, such a procedure can be performed in a straightforward manner using standard inverse fitting techniques. Once A and b are determined, they can be input back into Eq. (3) to obtain μ_{eff} (and hence μ_a) at every wavelength.

The above analysis demonstrates that the combination of point radiance spectroscopy (PRS) data and the assumption of a power law dependence of scattering allow a mixture of chromophores in a turbid medium to be fitted as if the medium was nonscattering.

B. P3 approximation for radiance

Equation (6) was derived within the framework of the diffusion approximation. However, because the first-order modes of the RTE dominate the overall shape of the radiance profile, Eq. (6) is also relevant to media better described by higher-order solutions to the RTE.[9,12] For fitting biological tissues, we implemented an analytical P3 forward model, based on the work by Hull and Foster[13] for a point source in an infinite medium, to generate radiance L and fluence ϕ. The P3 model is a third-order Legendre polynomial expansion of the RTE and has been shown to be more accurate than the commonly used first-order diffusion (P1) approximation for describing radiance measurements in turbid media.[9]

In the P3 approximation, the solution for a point source in spherical geometry is[13]

$$L_{\mathrm{P3}}(r,\hat{s}) = P_o\sum_{l=0}^{3}\frac{2l+1}{4\pi}[C'h_l(-\nu^-)Q_l(-\nu^- r) + D'h_l(-\nu^+)Q_l(-\nu^+ r)]P_l(\hat{s}\cdot\hat{r}), \tag{7}$$

where ν^+ and ν^- are comparable to the effective attenuation coefficient, μ_{eff}, and reduced transport coefficient, $\mu_t' = \mu_a + \mu_s'$, respectively, in the P1 approximation.[9,13] In addition, the P_l are Legendre polynomials of order l that provide the angular shape of each Nth order radiance mode. The bracketed terms are the relative contribution of each mode. Equation (7) simplifies to Eq. (2) if the former is truncated to first order and the optical properties converge to the limits of the P1 approximation.[9]

As with the diffusion approximation the P3 model requires as input a detection distance, r, detection angles, $\theta = a\cos(\hat{s}\cdot\hat{r})$, and optical properties. Although the interpretation of the absorption coefficient μ_a in the P3 model is consistent with the diffusion approximation, similarity relations are required to relate the two higher-order moments of the Henyey–Greenstein (HG) phase function of the P3 approximation to the reduced scattering coefficient, $\mu_s' = \mu_s(1-g)$, employed in diffusion theory.[13] Here, the first-order moment,

g, is also known as the anisotropy factor and is the average cosine of the scattering angle. In all cases a HG phase function was assumed which has been shown to provide an adequate approximation of the phase function of biological tissues.[14]

C. Basis spectra and inversion algorithm

In biological tissues, a spectral signature of the various absorbing and scattering components yields insight regarding tissue composition, functional status, and microstructure state. The dependence of the optical properties on wavelength, λ, is denoted by $\mu_a(\lambda)$ and $\mu_s'(\lambda)$. These functions are fed into the P3 forward model to generate point fluence $\phi_{P3}[\mu_a(\lambda),\mu_s'(\lambda),r]$ or point radiance spectra $L_{P3}[\mu_a(\lambda),\mu_s'(\lambda),r,\theta]$. Note that, unlike fluence, the radiance is specified by an additional parameter, θ, which describes the angle at the radiance measurement location.

In the current work, we are interested in fitting relative measurements at a single point. Therefore, radiance measurements employed the ratio of $L_r[\mu_a(\lambda),\mu_s'(\lambda),r,\theta]=L_{P3}[\mu_a(\lambda),\mu_s'(\lambda),r,90°]/L_{P3}[\mu_a(\lambda),\mu_s'(\lambda),r,0°]$ at each sampled wavelength. The fluence measurements over the whole spectral range were normalized to the intensity at a selected wavelength, $\phi_r[\mu_a(\lambda),\mu_s'(\lambda),r]=\phi_{P3}[\mu_a(\lambda),\mu_s'(\lambda),r]/\phi_{P3}[\mu_a(\lambda_o),\mu_s'(\lambda_o),r]$. Here we use $\lambda_o=800$ nm as the chosen normalization wavelength.

To describe the wavelength dependence of μ_s', we utilized a modified version of the power law equation for scattering in turbid media for point reflectance fitting:[5]

$$\mu_s'(\lambda)=A\left(\frac{\lambda}{\lambda_o}\right)^{-b}, \tag{8}$$

where A is the value of μ_s' at λ_o and b is a medium dependent scattering power factor. Equation (8) was adapted from a form originally proposed by Mourant *et al.*[15] that has shown to be a reasonable description of the scattering spectrum of both biological tissues and tissue-simulating intralipid phantoms[5,15] with the b parameter possibly related to the average scatterer size.

The shape of the total absorption spectrum, $\mu_a(\lambda)$, is the combination of the spectral shapes of the chromophores in the medium of interest and their respective concentrations. Here we perform an analysis using deoxyhemoglobin, $\mu_{a,Hb}(\lambda)$, oxyhemoglobin, $\mu_{a,HbO_2}(\lambda)$, hemoglobin, and water, $\mu_{a,water}(\lambda)$. The hemoglobin basis spectra were obtained from the on-line collection of Prahl,[16] while the water spectra were taken from the works of Kou *et al.*[17] and Pope and Fry.[18] In this case the total absorption spectrum $\mu_a(\lambda)$ takes the form

$$\mu_a(\lambda)=[\mathrm{Hb}]_t\mu_{a,HbO_2}(\lambda)SO_2+[\mathrm{Hb}]_t\mu_{a,Hb}(\lambda)(1-SO_2)+C_{water}\mu_{a,water}(\lambda). \tag{9}$$

$[\mathrm{Hb}]_t$ is the total hemoglobin concentration (μM), SO_2 is the oxygen saturation, and C_{water} is the water concentration. Note that in Eq. (9) both $\mu_{a,Hb}(\lambda)$ and $\mu_{a,HbO_2}(\lambda)$ are millimolar absorption spectra ($\mathrm{cm}^{-1}/\mu\mathrm{M}$) that must be scaled by $[\mathrm{Hb}]_t$ (μM) while $\mu_{a,water}(\lambda)$ is the true absorption spectrum (cm^{-1}) with C_{water} in dimensionless units (between 0 and 1). Equation (9) is representative of the absorption spectra in the near-infrared wavelength range for typical biological tissues, which are dominated by oxygenated and deoxygenated blood and water.

The vector of unknown scattering (A,b) and absorption parameters $([\mathrm{Hb}]_t,SO_2,C_{water})$ is determined using a trust-region fitting MATLAB algorithm that finds the set of best fit parameters that minimizes the chi-square value, χ^2, between the measured and P3 generated forward spectra. Convergence is assumed when the resulting χ^2 value reaches a predefined set of statistical criteria in the MATLAB environment. Each free parameter was given equal χ^2 weight. Furthermore, a positivity constraint was employed during fitting with both SO_2 and water concentration constrained to between 0% and 100%. Since convergence to the true solution is dependent on the number of surrounding local minima, their value relative to the global minimum, and the proximity of the initial estimate to the true solution, all initial estimates were purposely made nonphysical (−3 for all parameters) to avoid bias.

D. Tissue-simulating phantom experiments

Experimental validation of the above theoretical trends was performed in turbid tissue-simulating intralipid phantoms composed of soy-bean fat emulsion, absorbing dye, and water. Here, the absorption basis spectra are a linear combination of water, $\mu_{a,water}(\lambda)$, and naphthol green dye, $\mu_{a,naphthol}(\lambda)$: $\mu_a(\lambda)=C_{water}\mu_{a,water}+C_{naphthol}\mu_{a,naphthol}(\lambda)$, where $\mu_{a,water}(\lambda)$ was known from literature values and $\mu_{a,naphthol}(\lambda)$ was determined by measurement in a spectrophotometer without intralipid. In all cases, the chromophore spectral constraints were directly incorporated into the fitting procedure. We utilized equations derived by van Staveren *et al.*[19] to estimate the appropriate intralipid concentration to give a desired A value.

A spherical emitting fiber with an 850 μm diameter tip was coupled to a mercury arc lamp, serving as a broadband optical source. Radiance measurements were collected by a right angle microprism attached to a 600 μm multimode optical fiber coupled to a spectrometer.[8] The half angle acceptance cone of the radiance probe was measured to be 13.5° in water. The probe was attached to a precision rotational stage with 0.5° angular resolution, allowing for radiance measurements at various angles. The average of three readings, $L_{expt}(\lambda,\theta)$, were taken at 0° and two readings at the +90° and −90° positions. All measurements were background subtracted, wavelength corrected for lamp output, and normalized to the radiance reading at 710 nm to give $\kappa_r(\lambda,0°)$ and $\kappa_r(\lambda,90°)$ [Eq. (4)]. 710 nm was chosen because it lies approximately in the middle of the spectral measurement range. The two measurements, $L_{expt}(\lambda,0°)$ and $L_{expt}(\lambda,90°)$, were also divided to provide the experimental radiance ratio, $L_{rel,expt}(\lambda)$ [Eq. (2)]. Interstitial radiance measurements were recorded at a single optode separation ($r_o=4$ mm or $r_o=7.5$ mm).

To examine the ability of the PRS algorithm to determine chromophore concentrations, small aliquots of dye

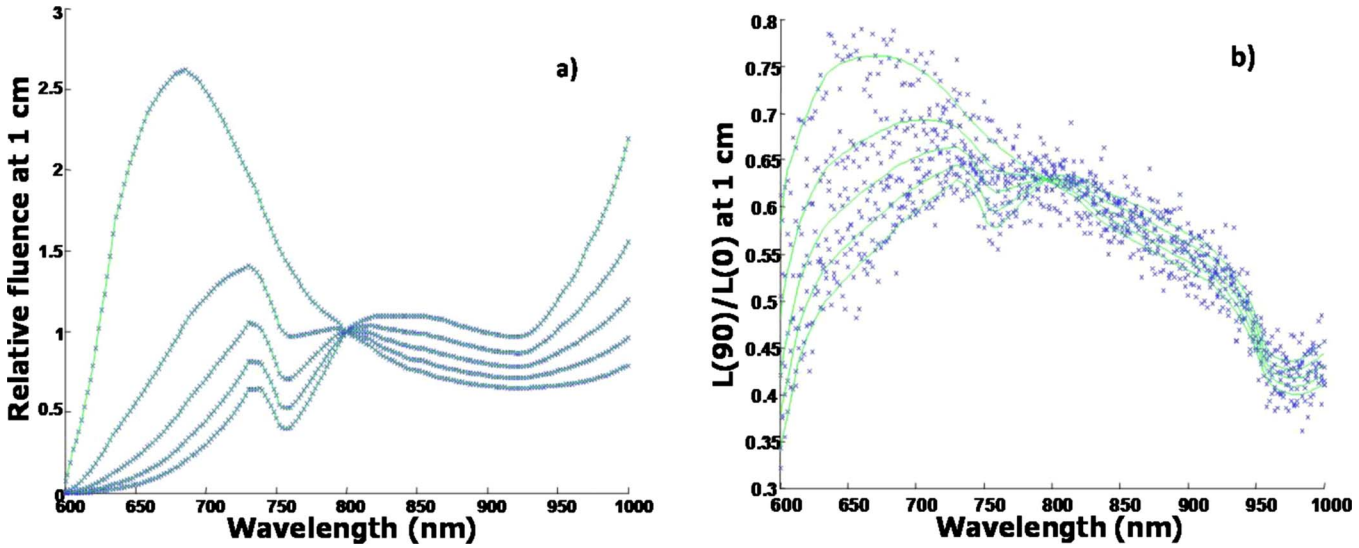

FIG. 2. (Color online) Representative fits of simulated relative (a) point fluence and (b) point radiance at various oxygen saturations (0–1 in increments of 0.25) at a fixed $[\mathrm{Hb}]_t$ of 100 μM. Crosses are the forward generated spectra while the solid lines are the resulting fits. The fluence spectra were generated under noise-free conditions with no water, while the radiance spectra were generated with 1% added noise and with the added presence of water (100% concentration).

were added to the intralipid phantoms. An ~0.4% concentration of 20% intralipid was employed for our base-line phantom.

The radiance spectrum was measured following each dye increment. Here, A is expected to remain constant (~9 cm^{-1}) as the dye is only absorbing (i.e., provides no scattering contribution). The maximum μ_a value measured at the highest concentration was ~3 cm^{-1} at 730 nm and is in the upper range of absorption for typical biological tissues.

The collected measurements were fitted to extract the unknown scattering parameters (A,b) and chromophore concentrations $(C_{\mathrm{water}}, C_{\mathrm{naphthol}})$ using a Levenberg–Marquardt fitting algorithm. During the fit, the parameters $(A,b,C_{\mathrm{water}},C_{\mathrm{naphthol}})$ were varied until a set of $\kappa_r(\lambda,0°)$, $\kappa_r(\lambda,90°)$, and $L_{\mathrm{rel}}(\lambda)$ was found that matched the experimental measurements to within the convergence criterion of the fitting algorithm. Note that we do not consider the effects of the finite numerical aperture (NA) of our radiance sensor in our forward model. Previous work by Dickey *et al.*[8] has indicated that NA does not need to be considered for accurate optical property recovery. This has been confirmed in our laboratory by a sensitivity analysis using the P3 approximation (to be published). To ensure physically relevant values, all parameters were constrained to values greater than zero, with the water concentration also constrained values to below or equal to 100%.

III. RESULTS

A. Uniqueness of spectrally resolved point fluence and radiance measurements

To verify Eq. (6), a systematic analysis was performed to evaluate the uniqueness of spectrally constrained point radiance, L_r, or point fluence, ϕ, measurements for inversely determining chromophore concentrations and scattering properties in turbid media. Using the P3 approximation, we generated a series of synthetic test spectra for both point ϕ and L_r data at a single location, and then applied the same P3 forward model to inversely fit for the unknown parameters. We should emphasize that the purpose of this work was not to verify the accuracy of the P3 model; in fact, this has already been done with experimental measurements (Sec. III B). Instead, we utilized the same P3 model to evaluate the uniqueness of the recovered optical parameters for point fluence and point radiance measurements. In this case, using the same model is appropriate as we are only evaluating the ability of a particular measurement to uniquely retrieve a desired optical parameter in the presence of noise. The spectra were generated between 600 and 1000 nm in 2 nm intervals assuming a turbid medium composed of oxy- and deoxyhemoglobin ranging from 20 to 120 μM at 20 μM resolution and at oxygen saturations between 0 and 1 in increments of 0.25. Scattering spectra used a μ_s' of 7.5 cm^{-1} (at 775 nm) and a b of 1.5. For the purposes of this analysis, the water spectrum was added primarily to confound the recovery of (A,b) and $(C_{\mathrm{Hb}},\mathrm{SO}_2)$ and, as such, was set artificially high to $C_{\mathrm{water}}=100\%$.

To emphasize the added information content of point radiance measurements compared to point fluence measurements, forward spectra were generated in two different ways. Fluence spectra were generated assuming noise-free conditions and with no water, thereby representing best case experimental conditions. Here a global minimum is expected for the fluence data at the true solution since all forward generated spectra were fitted using the same model. Radiance spectra were generated with 1% added noise and with water, thereby mimicking realistic experimental conditions. Preliminary experimental measurements using a spectrometer at similar sensor positions in intralipid phantoms with similar optical properties (μ_a ranging from 0 to 3 cm^{-1} and $\mu_s' \sim 7.5$ cm^{-1}) typically demonstrated much lower noise levels than the 1% tested in our simulations (data not presented). Therefore, the study evaluates the inherent informa-

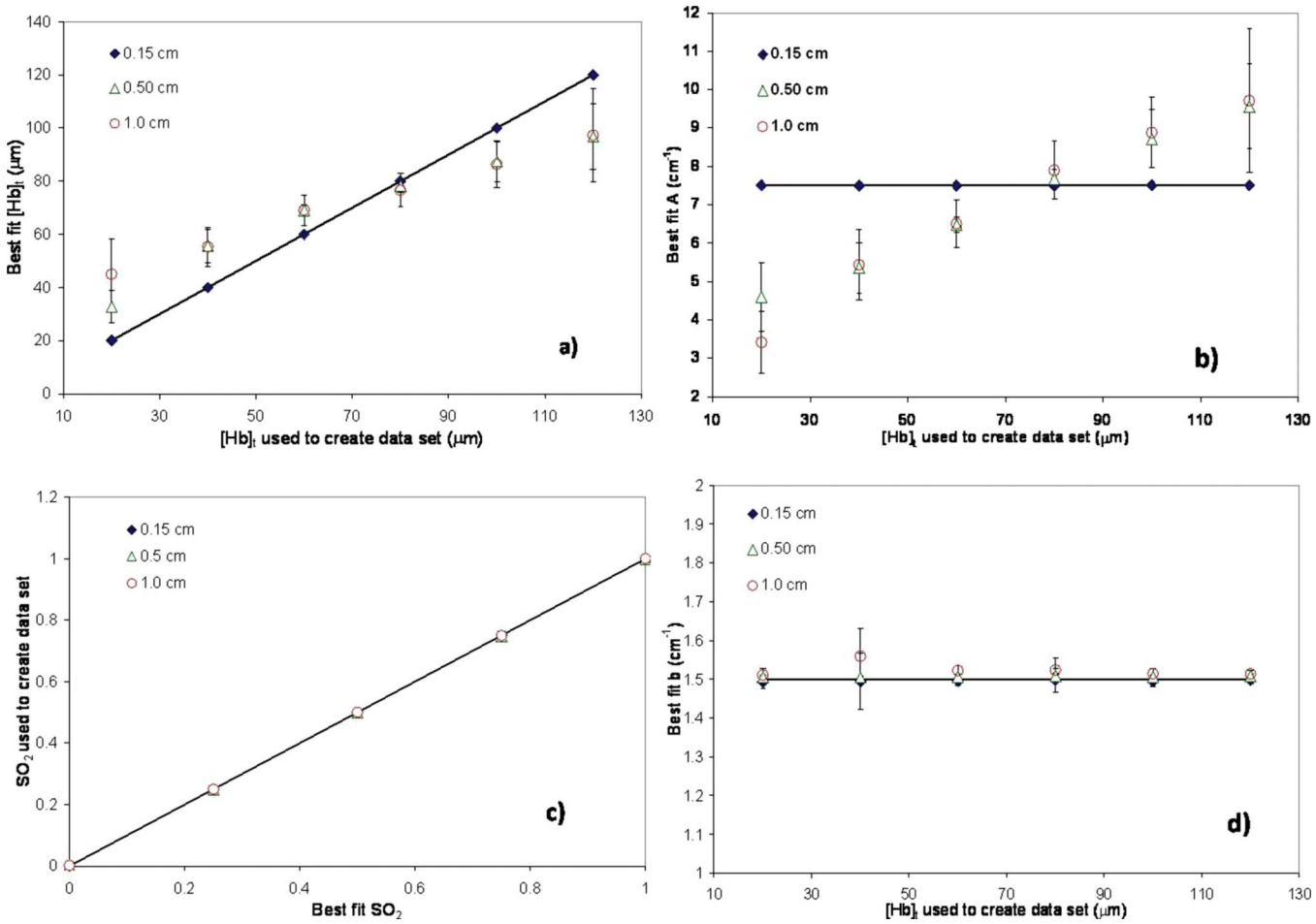

FIG. 3. (Color online) Best fit (a) $[\mathrm{Hb}]_t$, (b) A, (c) SO_2, and (d) b obtained by fitting relative point fluence spectra (normalized to 700 nm) as a function of hemoglobin concentration (μM) [(a), (b), and (d)] or SO_2 (c) used to create the simulated data. Solid lines indicate perfect agreement.

tion content and uniqueness of point fluence spectra while demonstrating the practical implementation of PRS.

Figure 2(a) shows sample forward spectra for point fluence (crosses) along with their associated best fit lines for a fixed $[\mathrm{Hb}]_t$ of 100 μM, A of 7.5 cm^{-1}, b of 1.5, and SO_2 ranging from 0 to 1 in 0.25 increments. Note that excellent agreement was obtained between the fitted and forward generated fluence data, which was representative of all oxygen saturations and hemoglobin saturations performed in the analysis. Figures 3(a) and 3(b) demonstrate that despite the excellent fits to the forward data as seen in Fig. 2(a), the spectral algorithm is unable to accurately recover $[\mathrm{Hb}]_t$ and A at the 0.5 and 1 cm sensor positions. Furthermore, an overestimation of $[\mathrm{Hb}]_t$ is mirrored by a corresponding decrease in A. Because the combination of these parameters determines the magnitude of the optical attenuation at each wavelength, it would appear that the systematic discrepancy in these parameters is a result of optical similarity which combines the effects of absorption and scattering into a single attenuation parameter; $\mu_{\mathrm{eff}}=\sqrt{3\mu_a(\mu_a+\mu_s')}$.[20] Interestingly, despite the limitations in absolute optical property recovery ($A\sim\mu_s'$, $[H_b]_t\sim\mu_a$), the algorithm is able to accurately recover SO_2 and b to within 0.0029% and 3%, respectively. The results confirm that under conditions of optical similarity (e.g., greater than two to three mean free paths from the source), point fluence measurements are unable to assess $[\mathrm{Hb}]_t$ and A parameters associated with absolute optical properties. This is consistent with fits at the 0.15 cm position (where optical similarity should not apply), where the fluence measurements provided recovery of all parameters to within ~0.04%. Finlay and Foster[4] previously reported recovery of absolute chromophore concentrations using multispectral constraints in reflectance geometry at similar *s-d* separations, although their algorithm, unlike our interstitial geometry results, was unable to recover absolute scattering coefficients.

Similar to the fluence data, Fig. 2(b) demonstrates sample forward spectra for point radiance (crosses) along with their associated best fit lines using the same input parameters as the fluence spectra. Again, reasonable agreement is obtained between the forward and fitted data. However, in contrast to the point fluence measurements, Figs. 4(a)–4(d) demonstrate that point radiance information is able to accurately recover all optical parameters typically to within ~10%, with the worst deviation occurring for the 0.15 cm position and 20 μM $[\mathrm{Hb}]_t$ concentration (~24% for $[\mathrm{Hb}]_t$ and ~0.1 absolute offset in SO_2). Furthermore, although not shown in Fig. 4, the water concentration was recovered to better than 10%. Interestingly, while the radiance technique appears to suffer from greater errors close to the source the

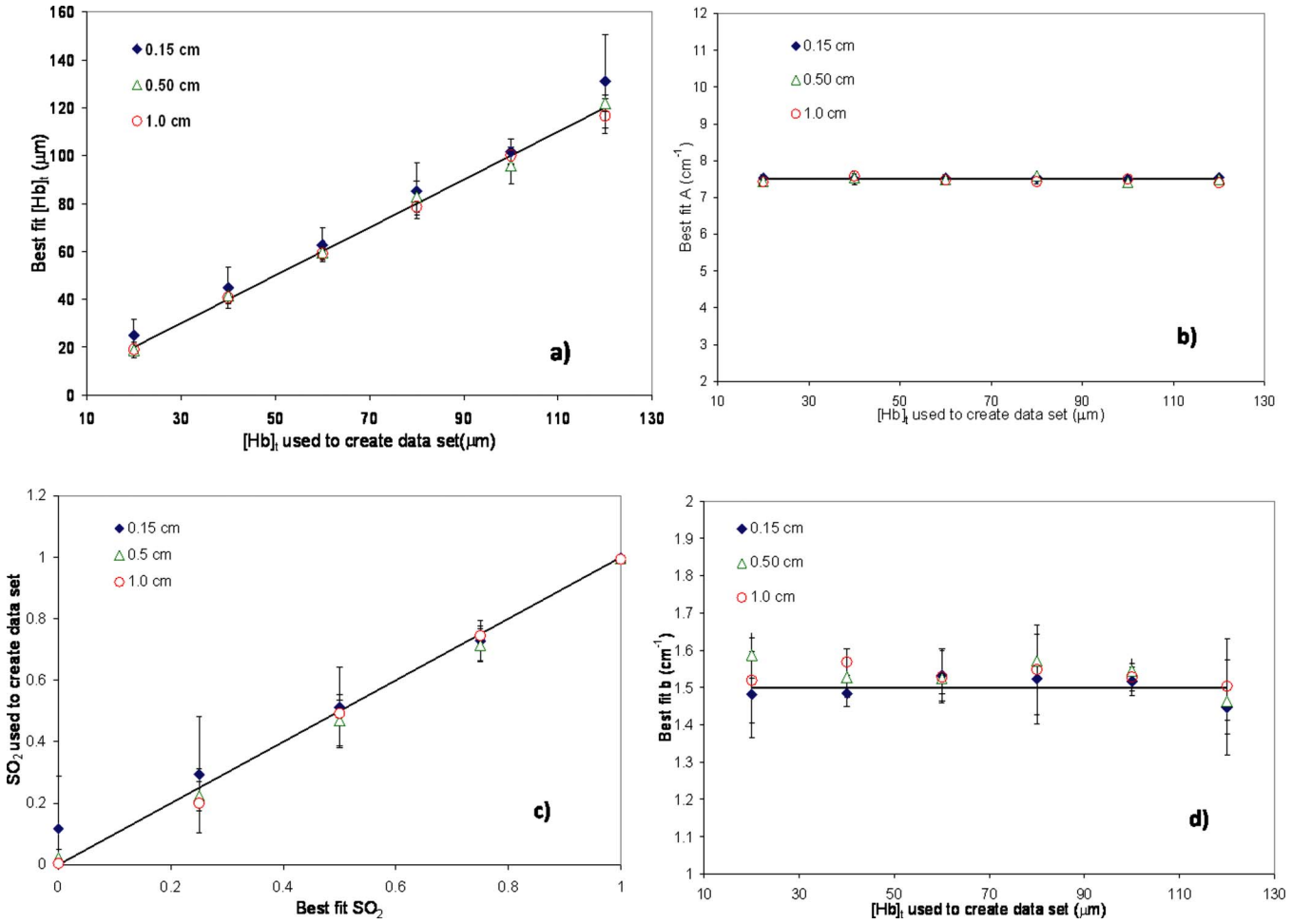

FIG. 4. (Color online) Best fit (a) $[\mathrm{Hb}]_t$, (b) A, (c) SO_2, and (d) b obtained by fitting relative point radiance ratio spectra, $L_r=L(90°)/L(0°)$, as a function of hemoglobin concentration [(a), (b), and (d)] or SO_2 (c) used to create the simulated data. Solid lines indicate perfect agreement.

fluence technique appears to become more robust. Again, note that unlike fluence, radiance simulations were performed with 1% noise and with the additional presence of the water spectrum [shown in Fig. 2(b)]. This indicates that point radiance information provides an inherently well-posed inverse problem even under realistic experimental conditions, while point fluence information is unable to achieve accurate determination of optical parameters even under ideal conditions.

We also evaluated the ability of the algorithm to retrieve scattering parameters with the aim of employing PRS for quantitative on-line monitoring of thermal coagulation during interstitial thermal therapies.[21] Another set of test spectra was generated to evaluate the sensitivity of point radiance and fluence measurements to changes in the reduced scattering coefficient. In these cases A was varied between 5 and 30 cm^{-1} in 5 cm^{-1} increments. The particular range chosen is indicative of scattering changes expected due to thermal coagulation of tissues.[22] Oxygen saturation was varied between 0 and 1 in 0.25 increments while the hemoglobin concentration was held constant at 100 μM.

As shown in Fig. 5(a), particularly at the 0.5 and 1 cm *s-d* separations, point fluence measurements are unable to accurately retrieve the value of A at high scattering conditions ($A>15$ cm^{-1}) with errors as high as ~30%. Again, a systematic decrease/increase in hemoglobin concentration was observed when A was overestimated/underestimated (data not shown). As in the previous case, parameters related to spectral shape such as SO_2 and b were determined with greater accuracy (within 3%) compared to absolute parameters over the entire range studied. This provides further evidence that spectral constraints can carry inherent information regarding relative shape changes in the absorption and scattering spectrum of a turbid medium. On the other hand, examination of Fig. 5(b) demonstrates that point radiance measurements were able to determine A to within ~5% over the full range of A examined, with the greatest deviations occurring at the 1 cm sensor position and $A=25$ cm^{-1} (~10%). The above results suggest that PRS for a single-source-detector geometry is able to provide quantitative information on optical scattering parameters typical of tissue in the visible and near infrared.

B. Experimental verification in tissue-simulating phantoms

As described in Sec. II D, experiments were performed to verify the point radiance spectroscopic technique. Figures 6(a) and 6(b) show the resulting radiance spectra (symbols) along with the corresponding fits (solid lines) for

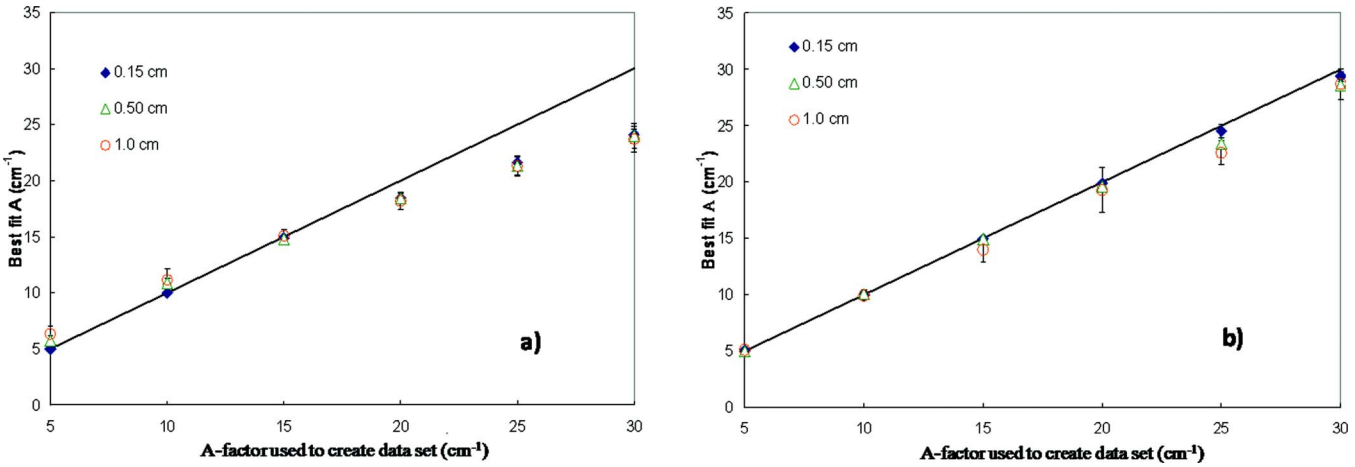

FIG. 5. (Color online) Best fit A obtained by fitting (a) relative point fluence (normalized to 700 nm) and (b) relative point radiance ratio spectra, $L_r = L(90°)/L(0°)$, as a function of A used to create the simulated data. Solid lines indicate perfect agreement.

$L(\lambda,0°)/L(\lambda,90°)$ and $\kappa_r(\lambda,0°)$, respectively, at 7.5 mm. Both fits demonstrate good agreement with the experimental data (with similar results at 4 mm, measurements not shown). Notice that $L(\lambda,0°)/L(\lambda,90°)$ in Fig. 6(a) gradually shifts to lower values with increasing absorption, reflecting the corresponding increase in anisotropy of the photon field as the phantom albedo decreases. Similarly, $\kappa_r(\lambda,0°)$ in Fig. 6(b) increases at the lower and upper wavelengths where the

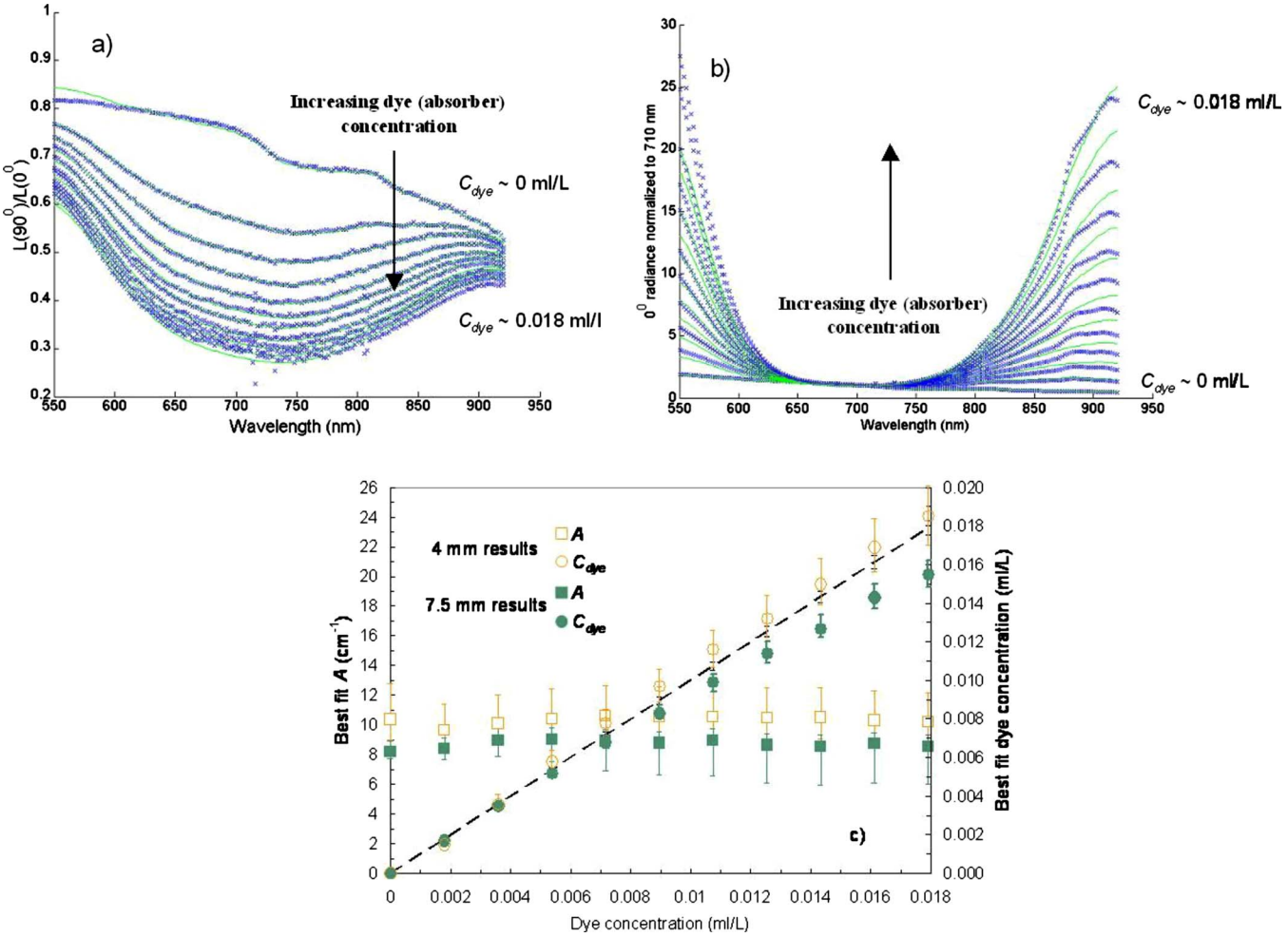

FIG. 6. (Color online) Typical (a) point radiance ratio $L(\lambda,0°)/L(\lambda,90°)$ [Eq. (2)] and (b) normalized $L(\lambda,0°)$ [$\kappa_r(\lambda,0°)$ from Eq. (4)] measured at 7.5 mm in an intralipid phantom as aliquots of naphthol green dye are added. The solid lines indicate the best fits of the P3 approximation for $L(\lambda,0°)/L(\lambda,90°)$ and $\kappa_r(\lambda,0°)$ to each spectrum. (c) Best fit A (left y-axis) and dye concentration (right y-axis) determined by simultaneously fitting $\kappa_r(\lambda,0°)$, $\kappa_r(\lambda,90°)$, and $L(\lambda,0°)/L(\lambda,90°)$ spectra acquired from intralipid phantoms with different concentrations of naphthol green dye. The dashed lines denote the theoretically expected result. Error bars are the recovered properties assuming ± 0.5 mm positioning error during fitting.

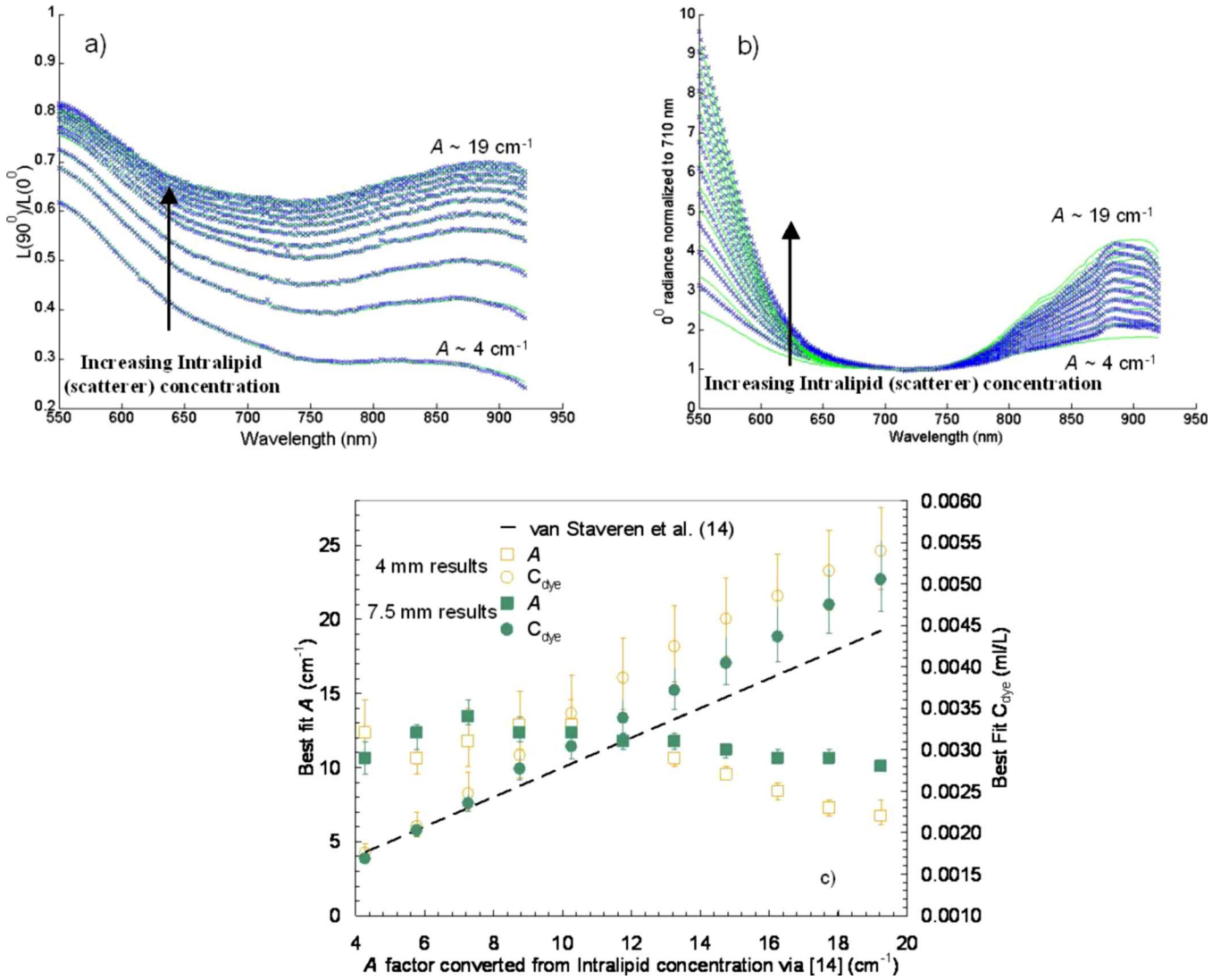

FIG. 7. (Color online) Typical (a) point radiance ratio $L(\lambda,0°)/L(\lambda,90°)$ [Eq. (2)] and (b) normalized $L(\lambda,0°)$ [$\kappa_r(\lambda,0°)$ from Eq. (4)] measured at 7.5 mm in an intralipid phantom as aliquots of additional intralipid are added. The solid lines indicate the best fits of the P3 approximation for $L(\lambda,0°)/L(\lambda,90°)$ and $\kappa_r(\lambda,0°)$ to each spectrum. (c) Best fit A (left y-axis) and dye concentration (right y-axis) determined by simultaneously fitting $\kappa_r(\lambda,0°)$, $\kappa_r(\lambda,90°)$, and $L(\lambda,0°)/L(\lambda,90°)$ spectra acquired in intralipid phantoms of different concentrations. The dashed line shows the A values as predicted by Jacques (Ref. 14).

absorption contribution of naphthol green is lower, indicating the increased attenuation of light near 775 nm (the naphthol green absorption peak) compared to the lower (near 550 nm) and upper (near 990 nm) wavelengths. Figure 6(c) displays the best-fit dye concentrations, C_{dye}, and A and demonstrates excellent retrieval of the absolute dye concentration (within ~10%) at both sensor positions over the entire range of concentrations. Notice that A remains virtually constant throughout, as was expected since the added dye is nonscattering. Small differences in recovered A at the 4 and 7.5 mm positions likely stem from variations in intralipid batches between separate phantoms.

A second set of experiments was performed to evaluate the sensitivity of PRS to scattering changes. An ~0.2% intralipid concentration (20% intralipid) was employed for our base-line phantom. Figures 7(a) and 7(b) show the resulting fits to the radiance spectra acquired as the scattering coefficient was increased by adding successive aliquots (~2 cm^{-1}/aliquot) of intralipid.[22] Again, good agreement with the experimental measurements was obtained. Note that, in this case, $L(90°)/L(0°)$ increases with added intralipid (scatterer), which is expected as the albedo increases and the medium becomes more diffuse. However, $\kappa_r(\lambda,0°)$ displays a similar trend as Fig. 6(b). Hence, while $L(90°)/L(0°)$ is sensitive to albedo differences, $\kappa_r(\lambda,0°)$ is sensitive to changes in attenuation. Because both increased scattering and absorption result in greater attenuation, the $\kappa_r(\lambda,0°)$ spectra are similar for both cases. This demonstrates the difficulty in recovering absolute optical properties using point relative attenuation measurements, thus emphasizing the improved information content of radiance over fluence measurements. Figure 7(c) shows the recovered A factor at both 4 and 7.5 cm positions as a function of intralipid concentration (converted to A using the analysis of van Staveren *et al.*[19]). Due to significant variations between different intralipid batches, we do not anticipate exact quantitative agreement in recovered A. However, as expected, a linear increase in scattering (dashed black lines) is observed

at both sensor positions as a function of added intralipid. Furthermore, C_{dye} remains relatively constant up to an A of $\sim 15\ cm^{-1}$. Discrepancies in predicted dye concentrations at higher intralipid concentrations may stem from optical property cross talk (due to optical similarity) during fitting, as the measured PRS data become increasingly similar in shape and magnitude [Figs. 7(a) and 7(b)].

The experimental results in Figs. 6 and 7 suggest that point radiance spectroscopic measurements are able to determine chromophore concentrations and scattering parameters independently and unambiguously over a range of optical properties and sensor positions typical of interstitial clinical applications.[23–25]

IV. DISCUSSION AND CONCLUSIONS

We have studied the role of spectrally constrained fitting of point optical data. We have shown that for point fluence measurements spectral constraints allow for the recovery of relative parameters (i.e., b and SO_2). Other authors have also suggested that recovery of SO_2 depends only weakly on the accurate recovery of *absolute* optical properties.[4,26] This is because fits of multispectral point fluence measurements are shape based and show the attenuation of light at different wavelengths relative to each other. On the other hand, our results indicate that families of solutions which generate the same relative attenuation (i.e., the same spectral shape) exist, thereby making absolute quantification impossible when utilizing point fluence data.

It should be noted that *spatially* resolved multispectral interstitial fluence measurements, which measure the effective attenuation coefficient at *each* wavelength and measure $\phi(r)$ at a variety of positions, have been utilized to determine absolute chromophore concentrations[1,4] and do not appear to suffer from the same issues of optical similarity as point fluence measurements. However, under the experimentally referred single-point detection conditions relative radiance measurements are able to uniquely separate absolute chromophore concentrations and A. This is because while relative fluence measurements are sensitive to attenuation, relative radiance measurements are more representative of the transport albedo yielding two inherently different sets of information. Previous studies by our group[9] have shown that for single wavelengths the absolute minimum in the χ^2 response is surrounded by a number of sparse local minima—making convergence to a unique set of optical properties difficult depending on noise conditions and sensor position. However, the addition of multiwavelength measurements combined with appropriate spectral constraints significantly improves the uniqueness of the inverse radiance fitting problem even in the presence of added noise.

Still the fact that point fluence measurements appear to provide absolute quantification of SO_2 and b suggests some interesting applications where absolute quantification is not necessary. For example, oxygen is a vital dosimetric parameter for determining the therapeutic outcome of photodynamic therapy.[27] Hence, while unable to provide an absolute measure of hemoglobin concentration, the point fluence approach may still prove a valuable tool for on-line photodynamic therapy monitoring. Similarly, the b parameter has been noted to be of value for noninvasive steady-state spectrally constrained optical tomography of breast tissues.[5] The same group has reported that if the value of b is known *a priori*, significant improvement in convergence was observed during reconstruction. In their work, prior knowledge of the population-averaged bulk values for b was utilized during inversion. However, our current work suggests that the b parameter can be measured directly from point fluence measurements prior to tomographic data collection, thereby providing more patient-specific information.

Of fundamental interest is the source of the uniqueness of relative radiance information. Time-domain methods, and by extension frequency-domain methods, rely on estimates of the optical pathlength by fitting a temporal distribution (or phase shift) of the photons arriving at a fixed source-detector distance to extract optical properties. Steady-state spatially resolved fluence techniques [$\phi(r)$ at several r's] rely on differences in the longer pathlengths traversed by photons far from the source (which are sensitive to absorption) and the shorter pathlengths traveled by photons close to the source (which are sensitive to scattering) to uniquely separate optical properties in turbid media. Since point radiance information provides similar quantification capabilities in the cw regime, it is possible that the radiance ratio is actually a representation of differences in average pathlength traveled between the two detection angles. For example, in the cases of very high absorption or no scattering, the radiance distribution will be highly forward directed. Conversely, in the case of no absorption or very high scattering, the forward and backward radiance is expected to be nearly equal. In this way, the transition between these two extremes provides information regarding the albedo of the medium being interrogated. Such information is unavailable from fluence measurements which are not sensitive to the directionality of the diffuse optical signal. Note that this principle is inherently different from the SDA method which requires *a priori* information of the water concentration to provide a normalization point for absolute quantification at a reference wavelength, with the spectral information employed to extrapolate the reference point to other wavelengths. With radiance, the information is inherent in the measurements, much like spatially resolved cw fluence measurements and time-domain methods.

The results of this study point toward the significant potential of PRS of turbid media. cw methods with similar capabilities to the point radiance approach require spatial scans over a larger volume that can typically provide only an average bulk assessment of the tissue state. On the other hand, local point reflectance measurements provide a regional determination of tissue properties. However, similar to traditional biopsies, such methods may miss a targeted disease if not positioned exactly in the intended location. The developed PRS technique offers a compromise between local reflectance and spatially resolved fluence techniques, as it can probe the volume between a single-source-detector pair at larger separations than local reflectance techniques. Until recently, the only other method capable of determining absolute tissue optical properties at similar single-source-detector

separations was a time-domain technique that required expensive pico- or femtosecond lasers and detectors with nanosecond resolution.

The ultimate goal of our work is to design a single simple and robust bundled probe composed of two fixed perpendicular radiance sensors. This would remove the necessity for time consuming and potentially technically challenging on-line rotations and allow both 0° and 90° radiance measurements to be acquired experimentally at the same instant, thereby allowing for quantification of temporally varying optical changes such as hemoglobin concentration or oxygen saturation. The same fibers may be employed as a local reflectance probe with one fiber employed as a source and the other fiber employed as a detector. Following local interrogation the point radiance technique can be employed to generate a semilocal measure of tissue properties. In addition, source-sensor pairs may be scanned spatially in parallel to provide a rough chromophore/scattering map of the targeted tissue. With proper development, PRS may provide another tool for interstitial spectroscopy of turbid media.

We note that although the method is derived for interstitial applications, with the advent of noncontact diffuse optical instrumentation that are able to measure the surface flux, the proposed method may potentially be extended to optical tomographic applications.[28,29]

ACKNOWLEDGMENTS

Financial support for this work was provided by the National Cancer Institute of Canada (with funds from the Canadian Cancer Society) and the Natural Sciences and Engineering Research Council of Canada. The authors would like to thank Dr. Brian Wilson, Dr. John Tulip, and Dr. Dwayne Dickey for helpful discussions and insight.

[1]T. C. Zhu, J. C. Finlay, and S. M. Hahn, J. Photochem. Photobiol., B **79**, 231 (2005).
[2]C. R. Buttemere, R. S. Chari, C. D. Anderson, M. K. Washington, A. Mahadevan-Jansen, and L. C. Lin, J. Biomed. Opt. **9**, 1018 (2004).
[3]A. Amelink, H. J. Sterenborg, M. P. Bard, and S. Burgers, Opt. Lett. **29**, 1087 (2004).
[4]J. C. Finlay and T. H. Foster, Med. Phys. **31**, 1949 (2004).
[5]A. Corlu, T. Durduran, R. Choe, M. Schweiger, E. M. Hillman, S. R. Arridge, and A. G. Yodh, Opt. Lett. **28**, 2339 (2003).
[6]P. R. Bargo, S. A. Prahl, T. T. Goodell, R. A. Sleven, G. Koval, G. Blair, and S. L. Jacques, J. Biomed. Opt. **10**, 034018 (2005).
[7]H. Xu, B. W. Pogue, H. Dehghani, K. Paulsen, R. Springett, and J. F. Dunn, Opt Lett. **29**, 2043 (2004).
[8]D. J. Dickey, R. B. Moore, D. C. Rayner, and J. Tulip, Phys. Med. Biol. **43**, 3559 (1998).
[9]L. C. L. Chin, W. M. Whelan, and I. A. Vitkin, Appl. Opt. **45**, 2101 (2006).
[10]S. Chandrasekhar, *Radiative Transfer* (Dover, New York, 1960).
[11]J. R. Mourant, T. Fusilier, J. Boyer, T. M. Johnson, and I. J. Bigio, Appl. Opt. **36**, 949 (1997).
[12]L. C. L. Chin, W. M. Whelan, A. E. Worthington, W. M. Whelan, and I. A. Vitkin, J. Biomed. Opt. **12**, 06402 (2007).
[13]E. L. Hull and T. H. Foster, J. Opt. Soc. Am. A **18**, 584 (2001).
[14]S. L. Jacques, Adv. Biomed. Photon. Imaging **2**, 364 (1996).
[15]J. R. Mourant, T. Fusilier, J. Boyer, T. M. Johnson, and I. J. Bigio, Appl. Opt. **36**, 949 (1997).
[16]S. A. Prahl, http://omlc.ogi.edu/spectra/hemoglobin/summary.html.
[17]L. Kou, D. Labrie, and P. Chylek, Appl. Opt. **32**, 3531 (1993).
[18]R. M. Pope and E. S. Fry, Appl. Opt. **36**, 8710 (1997).
[19]H. J. van Staveren, C. J. M. Moes, J. van Marle, S. A. Prahl, and M. J. C. van Gemert, Appl. Opt. **30**, 4507 (1991).
[20]D. R. Wyman, M. S. Patterson, and B. C. Wilson, Appl. Opt. **28**, 5243 (1989).
[21]L. C. L. Chin, B. C. Wilson, W. M. Whelan, and I. A. Vitkin, Opt. Lett. **29**, 959 (2004).
[22]J. P. Ritz, A. Roggan, C. Isbert, G. Muller, H. J. Buhr, and C. T. Germer, Lasers Surg. Med. **29**, 205 (2001).
[23]H. Xu and M. S. Patterson, Opt. Express **14**, 6485 (2006).
[24]J. Siewerdsen, D. J. Mosely, S. Burch, S. K. Bisland, A. Bogaards, B. C. Wilson, and D. A. Jaffray, Med. Phys. **32**, 241 (2005).
[25]W. M. Whelan, P. Chun, L. C. Chin, M. D. Sherar, and I. A. Vitkin, Phys. Med. Biol. **46**, N91 (2001).
[26]V. Ntziachristos, M. Kohl, H. Ma, and B. Chance, Med. Phys. **27**, 410 (2000).
[27]T. H. Foster, D. F. Hartley, M. G. Nichols, and M. R. Hilf, Cancer Res. **53**, 1249 (1993).
[28]J. Ripoll, R. B. Schulz, and V. Ntziachristos, Phys. Rev. Lett. **91**, 103901 (2003).
[29]J. Ripoll and V. Ntziachristos, Phys. Rev. Lett. **96**, 173903 (2006).